The targeted cytosolic degradation of class I histone deacetylases is essential for efficient alphaherpesvirus replication

Sheng-Li Ming[1,2,3#], Meng-Hua Du[1,2,3#], Jia-Ming Yang[6#], Ya-Di Guo[1,2,3], Jia-Jia Pan[1,2,3], Wei-Fei Lu[1,2,3], Jiang Wang[1,2,3,5], Lei Zeng[1,2,3*], Bei-Bei Chu[1,2,3,4,5*]

[1]College of Veterinary Medicine, Henan Agricultural University, Zhengzhou 450046, Henan Province, China

[2]Key Laboratory of Animal Biochemistry and Nutrition, Ministry of Agriculture and Rural Affairs, China

[3]Key Laboratory of Animal Growth and Development of Henan Province, Henan Agricultural University, Zhengzhou 450046, Henan Province, China

[4]International Joint Research Center of National Animal Immunology, Henan Agricultural University, Zhengzhou 450046, Henan Province, China

[5]Ministry of Education Key Laboratory for Animal Pathogens and Biosafety, Zhengzhou 450046, Henan Province, China

[6]State Key Laboratory of Membrane Biology, School of Pharmaceutical Sciences, Tsinghua University, Beijing 100084, China

[#]These authors contributed equally

[*]Correspondence: zenglei@henau.edu.cn (L. Zeng); chubeibei@henau.edu.cn (B.-B. Chu).

Abstract

Viral infection triggers a robust DNA damage response (DDR), reshaping the host chromatin landscape to facilitate viral replication. Here, we uncover a novel mechanism by which alphaherpesviruses exploit the DDR pathway. We demonstrated that herpes simplex virus 1 (HSV-1) and pseudorabies virus (PRV) induced selective degradation of class I histone deacetylases (HDAC1/2), leading to histone hyperacetylation and subsequent DDR activation. Strikingly, viral infection promoted nuclear export of HDAC1/2, followed by MDM2-mediated K63-linked polyubiquitination and proteasomal degradation in the cytoplasm. Pharmacological inhibition of either DDR signaling or HDAC1/2 nuclear export significantly affected viral replication *in vitro* and *in vivo*. Our findings reveal a unique viral strategy to hijack host epigenetic regulation for efficient replication and identify potential therapeutic targets for alphaherpesvirus infections.

Keywords: Alphaherpesviruses; HDACs; MDM2; Ubiquitination; DNA damage response.

Introduction

HSV-1 is a widespread neurotropic virus that infects more than two-thirds of the global population under the age of 50[1]. After initial infection of mucosal epithelia and neuronal tissues, HSV-1 establishes lifelong latency within sensory ganglia[2]. Clinically, HSV-1 infection can present as oral or genital lesions and, in severe instances, may progress to herpes simplex encephalitis—a potentially fatal inflammation of the brain[3, 4]. Emerging evidence suggests a plausible association between HSV-1 and neurodegenerative conditions such as Alzheimer's disease, linking chronic neuroinflammation and neuronal impairment to persistent viral infection[5, 6]. To sustain lifelong infection, HSV-1 employs sophisticated strategies to evade host immune defenses and maintain latent reservoirs.

Epigenetic regulation plays a critical role in governing HSV-1 latency and reactivation[7, 8]. During latency, the virus coopts host histone deacetylases (HDACs) to enforce viral genomic silencing through chromatin condensation[9]. Although HDAC1 and HDAC2 are central to chromatin stability and DNA damage response (DDR), their roles during alphaherpesvirus infection appear complex and context-dependent[10]. While these enzymes contribute to viral repression during latency[11], their potential involvement in promoting lytic replication—whether through degradation or functional inactivation—has remained inadequately explored.

Histone acetylation, a pivotal epigenetic modification that modulates chromatin accessibility and transcriptional activity, is dynamically regulated by histone acetyltransferases (HATs), which add acetyl groups to activate gene expression, and HDACs, which remove these groups to enforce repression[12, 13]. The HDAC family is categorized into four classes: Class I (HDAC1, 2, 3, 8), Class IIa/b, Class III (sirtuins), and Class IV (HDAC11)[14]. Among these, Class I HDACs—particularly HDAC1 and HDAC2—are indispensable for chromatin remodeling, genomic integrity, and immune modulation[15-18]. These enzymes contribute to host antiviral defense by fine-tuning the expression of immune-related genes. Nevertheless, the mechanisms through which HSV-1 overcomes this transcriptional repression remain incompletely understood[18].

HDAC1 serves as a key regulator of chromatin dynamics and innate immune signaling, interfacing with critical pathways such as NF-κB, JAK-STAT, and Toll-like receptor cascades to shape antiviral responses[19-22]. For example, in lung epithelial cells, HDAC1 facilitates STAT1 phosphorylation and enhances interferon-stimulated gene (ISG) activation, thereby restricting influenza A virus replication[23]. This underscores the dual function of HDAC1 in both epigenetic control and immune regulation. However, the specific strategies used by HSV-1 to manipulate HDAC1/2—particularly through ubiquitin-mediated degradation—to circumvent host immunity and enhance viral replication have not been clearly defined.

This study reveals that HSV-1 induces the degradation of HDAC1/2 via an MDM2-dependent ubiquitination mechanism, resulting in elevated histone acetylation, chromatin relaxation, and activation of DNA damage response pathways that collectively enhance viral replication. These findings offer novel insights into the epigenetic subversion strategies employed by HSV-1 and underscore the therapeutic potential of targeting the HDAC–MDM2 axis in the treatment of herpesvirus infections.

Materials and Methods

Mice

Female C57BL/6J mice (6–8 weeks old) were purchased from the Experimental Animal Center of Zhengzhou University (Zhengzhou, China) and housed in specific-pathogen-free facilities under controlled environmental conditions, including a 12-hour light-dark cycle and a temperature of 22°C. For in vivo infection studies, mice were anesthetized with isoflurane prior to intranasal inoculation with HSV-1, at a dose of 1×10^6 PFU per mouse in a total volume of 30 μL PBS. Clinical signs—including ruffled fur, hunched posture, reduced mobility, and body weight loss 15%—were monitored daily. On day 15 post-infection, mice were humanely euthanized by intravenous injection of sodium pentobarbital (90 mg/kg), following the "Guidelines for the Euthanasia of Laboratory Animals". Immediately thereafter, tissues—including liver, spleen, lung, brain, and

99 draining cervical lymph nodes—and serum were harvested under sterile conditions. All
100 tissues were snap-frozen in liquid nitrogen within 60 seconds of excision and stored at
101 −80°C until further analysis. Samples were processed for Western blotting. All
102 procedures were in accordance.

103 **Reagents and plasmids**

104 Reagents were sourced as follows: Leptomycin B (HY-16909), MG-132 (HY-13259),
105 3-MA (HY-19312), cycloheximide (HY-12320), and chloroquine (HY-17589A) were
106 purchased from MedChemExpress; berzosertib (S7102) was purchased from Selleck;
107 DMSO (W387520) was purchased from Sigma-Aldrich. Unless otherwise specified, all
108 inhibitors were added at 1 hour post-infection (hpi), after completion of viral adsorption
109 and entry, to avoid interference with early viral processes. Antibodies against CHK1
110 (25887-1-AP), CHK2 (13954-1-AP), RAD51 (14961-1-AP), β-actin (66009-1-lg), P53
111 (10442-1-AP), HDAC1 (10197-1-AP), HDAC2 (12922-3-AP), HDAC4 (17449-1-AP),
112 HDAC6 (12834-1-AP), HDAC11 (67949-1-Ig), and EGFP (50430-2-AP) were
113 purchased from Proteintech; antibodies against p-P53 (9286), p-ATM (13050), ATM
114 (2873), ATR (13934), p-ATR (2853), p-CHK1 (12302), p-CHK2 (2197), γ-H2AX
115 (80312), H3 (4499), H4K8ac (2594), H4K12ac (13944), H4 (13919), H2AX (7631),
116 H3K9ac (4658), H3K27ac (8173), UB (20326), and MDM2 (86934) were purchased
117 from Cell Signaling Technology; H3K56ac antibody (07-677) was purchased from
118 Millipore; ICP4 antibody (ab6514) was purchased from Abcam; ICP0 antibody (sc-
119 53070) was purchased from Santa Cruz Biotechnology; FLAG antibody (F7425) was
120 purchased from Sigma-Aldrich; HA antibody (A00169) was purchased from GenScript.

121 HDAC1 and HDAC2 coding sequences were amplified from HEK293 cell cDNA and
122 cloned into p3×FLAG-CMV-10 to generate FLAG-tagged expression constructs.
123 MDM2 coding sequence was amplified and inserted into pEGFP-C1 to produce EGFP-
124 MDM2. Site-directed mutagenesis was performed using the QuikChange Site-Directed
125 Mutagenesis Kit (Agilent Technologies, 200523) per the manufacturer's instructions to
126 generate: FLAG-HDAC1 K8R, FLAG-HDAC1 K10R, FLAG-HDAC1 K31R, FLAG-
127 HDAC1 K50R, FLAG-HDAC1 K58R, FLAG-HDAC1 K66R, FLAG-HDAC1 K74R,

128 FLAG-HDAC1 K89R, FLAG-HDAC2 K75R, FLAG-HDAC1 (aa 1–329), FLAG-
129 HDAC1 (aa 329–482), FLAG-HDAC1 (aa 1–100), FLAG-HDAC1 (aa 100–329),, and
130 EGFP-MDM2ΔRING (aa 1–435). FLAG-HDAC1 ΔNES (residues 207–216 deleted),
131 in which the deletion encompasses the CRM1-dependent nuclear export signal as
132 predicted by NESmapper. HA-tagged ubiquitin constructs [HA-UB (WT), HA-UB
133 (K48), HA-UB (K63)] were provided by Dr. Bo Zhong (College of Life Sciences,
134 Wuhan University, China).

135 **Cells**

136 Cell lines (HeLa/ATCC CL-82, Vero/ATCC CL-81, 3D4/21/ATCC CRL-2843,
137 HEK293T/ATCC CRL-11268) were cultured in DMEM or RPMI 1640 supplemented
138 with 10% fetal bovine serum (FBS), 1% penicillin/streptomycin, and 1% L-glutamine
139 at 37°C under 5% CO_2 in a humidified incubator. For transient transfections, DNA
140 constructs were delivered to HeLa and HEK293T cells using Lipofectamine 3000
141 (Invitrogen, L3000001) per the manufacturer's protocol.

142 To generate shRNA-mediated knockdown cell lines, HEK293T cells were co-
143 transfected with control or gene-specific shRNA (Table S1), packaging plasmid
144 psPAX2, and envelope plasmid pMD2.G. Post-transfection (6 h), medium was replaced,
145 and lentiviral particles were harvested at 48 hours. Parental cells were infected with
146 viral supernatant and selected with puromycin to establish stable knockdown lines.

147 To generate siRNA-mediated knockdown cell lines, HeLa cells were transfected with
148 either a non-targeting control siRNA or gene-specific siRNAs (Table S1) using
149 Lipofectamine™ RNAiMAX(Invitrogen, 13778030). Transfection was performed at a
150 confluency of approximately 30%, and target gene and protein expression levels were
151 assessed 48 hours post-transfection.

152 **Viruses**

153 HSV-1 strain F (provided by Dr. Chun-Fu Zheng, University of Calgary, Canada) and
154 PRV-QXX were propagated per established protocols [24]. Viral titers were determined
155 by plaque assays in Vero cells. For in vitro infections, cells were infected with HSV-1

156 or PRV-QXX at an MOI of 1. For in vivo studies, mice were intranasally inoculated
157 with HSV-1 (1×10^6 pfu/mouse).

158 **Immunoblotting, ubiquitination and Co-immunoprecipitation** (Co-IP)

159 For immunoblotting, cells were lysed in RIPA buffer [50 mM Tris-HCl (pH 8.0), 150
160 mM NaCl, 1% Triton X-100, 1% sodium deoxycholate, 0.1% SDS, 2 mM $MgCl_2$]
161 supplemented with protease/phosphatase inhibitors. Proteins were resolved by SDS-
162 PAGE, transferred to PVDF membranes, and blocked with 5% nonfat milk in TBST (1
163 hour, RT). Membranes were incubated with primary antibodies (overnight, 4°C), then
164 HRP-conjugated secondary antibodies (1 hour, RT). Signals were detected using
165 Laminate Crescendo Western HRP Substrate (Millipore, Cat. No. WBLUR0500) on a
166 GE AI600 imager.

167 For ubiquitination assay, cells were lysed in IP buffer [50 mM Tris-HCl (pH 7.4), 150
168 mM NaCl, 1% NP-40, 1% sodium deoxycholate, 5 mM EDTA, 5 mM EGTA] and
169 clarified (16,000 × *g*, 10 minutes, 4°C). Subsequently, 900 µl aliquots were incubated
170 with 40 µl of a 1:1 slurry of Sepharose beads conjugated to anti-HDAC1 or anti-FLAG
171 mouse monoclonal antibodies (4°C, 4 hours). Beads were washed four times with IP
172 buffer, eluted in SDS sample buffer (10 minutes, boiling), and analyzed by
173 immunoblotting.

174 For Co-IP assay, cells were lysed in Co-IP buffer [50 mM Tris-HCl (pH 7.4), 150 mM
175 NaCl, 1% NP-40, 5 mM EDTA, 5 mM EGTA] and clarified (16,000 × *g*, 10 minutes,
176 4°C). Aliquots (900 µl) were incubated with 40 µl of a 1:1 slurry of Sepharose beads
177 conjugated to IgG (GE Healthcare) or anti-FLAG mouse monoclonal antibody (4°C, 4
178 hours). Beads were washed three times with Co-IP buffer, eluted in SDS sample buffer
179 (10 minutes, boiling), and analyzed by immunoblotting.

180 **Immunofluorescence assay**

181 Cells were fixed in 4% paraformaldehyde at room temperature for 20 min on coverslips
182 in 12-well plates. Following three washes with PBS, cells were permeabilized with 0.2%
183 Triton X-100 for 20 min and subsequently blocked with 10% FBS. Specific primary

184 antibodies, diluted in 10% FBS, were then applied to the cells and incubated for 1 h at
185 room temperature. After three PBS washes, cells were exposed to the appropriate
186 secondary antibodies, also diluted in 10% FBS, for 1 h at room temperature. Nuclei
187 were stained with DAPI for 5 min at room temperature, mounted using Prolong
188 Diamond (Invitrogen), and visualized using a Zeiss LSM 800 confocal microscope.

189 **Comet assay**

190 Cells were seeded in 6-well plates and treated accordingly. Frosted microscope slides
191 were coated with 0.5% normal melting point agarose. A mixture of 10 μL DMEM
192 containing around 10,000 cells and 75 μL of 0.7% low melting point agarose was
193 layered onto the pre-coated agarose. An additional 75 μL of 0.7% low melting point
194 agarose formed a third layer. The slides were lysed in a buffer containing 10 mM Tris-
195 HCl, pH 10.0, 2.5 M NaCl, 100 mM Na2EDTA, 1% Triton X-100, and 10% DMSO for
196 2 hours at 4°C. Post-lysis, the slides were treated with an electrophoresis solution (300
197 mM NaOH, 1 mM Na2EDTA, pH >13) for 40 minutes, electrophoresed at 20 V (~300
198 mA) for 25 minutes, and neutralized with 0.4 mM Tris-HCl (pH 7.5). Subsequently,
199 cells were stained with propidium iodide (PI, 5 μg/mL) and examined using a Zeiss
200 LSM 800 confocal microscope. DNA damage was assessed based on tail moment using
201 CometScore software.

202 **qRT-PCR analysis**

203 Total RNA was isolated using TRIzol reagent (TaKaRa) and reverse-transcribed into
204 cDNA with the PrimeScript RT reagent kit (TaKaRa). qRT-PCR was performed in
205 triplicate using SYBR Premix Ex Taq (TaKaRa) according to the manufacturer's
206 protocol. Expression levels were normalized to β-actin as an internal reference. Melting
207 curve analysis confirmed amplification specificity by verifying single-product
208 formation in all reactions. Relative gene expression was calculated using the $2^{-\Delta\Delta Ct}$
209 method. Primer sequences are provided in Table S1

210 **Plaque assay**

211 Vero cells (seeded in six-well plates) were grown to confluence, infected with serially

212 diluted viruses (10^{-1}–10^{-7}; 1 hour, 37°C), and washed with PBS to remove residual
213 inoculum. DMEM containing 1% methylcellulose (4 mL/well) was added, and cells
214 were incubated for 4–5 days. Post-incubation, cells were fixed with 4%
215 paraformaldehyde (15 minutes), stained with 1% crystal violet (30 minutes), and
216 plaques were quantified.

217 **Statistical analysis**

218 Statistical analyses were performed using GraphPad Prism 8 software. Comparisons
219 between two groups were evaluated using a two-tailed Student's *t*-test. Significance
220 was defined as $P < 0.05$. Data are presented as mean ± SD of three independent
221 experiments. Kaplan-Meier survival curves were generated and analyzed for mouse
222 survival assessment.

223

224 **Results**

225 **HSV-1 infection promotes HDAC1/2 degradation and histone hyperacetylation.**

226 Post-translational modifications of histones play a critical role in regulating chromatin
227 remodeling and gene expression. HDACs, a highly conserved enzyme family [25],
228 catalyze the removal of acetyl groups from histones, thereby promoting chromatin
229 condensation and transcriptional repression. To investigate the effect of HSV-1
230 infection on HDAC expression and histone acetylation, we examined the protein levels
231 of key HDAC isoforms following viral infection. Immunoblotting analysis revealed a
232 marked decrease in HDAC1 and HDAC2 protein levels in cells infected with either
233 HSV-1 or PRV, whereas the expression of HDAC4, HDAC6, and HDAC11 remained
234 unchanged (Fig. 1A, B). In contrast, qRT-PCR results showed no alterations in HDAC1
235 and HDAC2 mRNA levels (Fig. 1C, D), suggesting that their depletion is regulated at
236 the post-translational level.

237 To assess the functional impact of HDAC1/2 reduction, we examined global histone
238 acetylation patterns. Site-specific immunoblotting demonstrated elevated acetylation at
239 multiple lysine residues, including H3K9, H3K27, H3K56, H4K8, and H4K12, in HSV-
240 1-infected HeLa cells (Fig. 1E). A similar hyperacetylation profile was observed in

241 PRV-infected 3D4/21 cells and in murine liver tissues infected with HSV-1 (Fig. 1F, G).
242 Next, we assessed the effect of HDAC1/2 knockdown on global histone acetylation and
243 observed significantly elevated acetylation at multiple evolutionarily conserved lysine
244 residues—including H3K9, H3K27, H3K56, H4K8, and H4K12—consistent with
245 genome-wide histone hyperacetylation (Fig. H). Together, these findings indicate that
246 HSV-1 selectively degrades class I HDACs, resulting in widespread histone
247 hyperacetylation that fosters a chromatin state conducive to viral replication.

248 **HSV-1 infection induces DDR through HDAC1/2 depletion and histone**
249 **hyperacetylation.**

250 Given that excessive histone acetylation can destabilize chromatin structure, we sought
251 to elucidate the mechanism by which this epigenetic modification activates the DDR
252 pathway. Accumulating evidence underscores the pivotal role of histone modifications
253 in maintaining genomic stability, with dynamic changes in chromatin architecture being
254 intimately associated with DDR initiation. To determine whether HSV-1 infection
255 induces DDR activation, we evaluated the phosphorylation of γ-H2AX, a well-
256 established marker of DNA double-strand breaks. Immunofluorescence microscopy
257 revealed a significant increase in γ-H2AX foci in cells infected with HSV-1 or PRV
258 (Fig. 2A-C). Comet assays (single-cell gel electrophoresis) quantify DNA
259 fragmentation, with an increased tail moment reflecting elevated levels of DNA
260 damage—findings that further corroborate enhanced DNA fragmentation under these
261 experimental conditions (Fig. 2D–G).Given the central role of ATM/ATR signaling in
262 the DDR, we proceeded to examine the activation of key checkpoint kinases.
263 Immunoblotting analysis confirmed phosphorylation of ATM, ATR, Chk1, Chk2,
264 H2AX, and RAD51 in HSV-1-infected HeLa cells and 3D4/21 cells (Fig. 2H, I).
265 Subsequently, we assessed the effect of HDAC1 knockdown on the DDR pathway and
266 found that HDAC1-depleted HeLa cells exhibited reduced phosphorylation of ATM,
267 ATR, and H2AX(Fig. 2J), providing initial evidence that HSV-1 infection promotes
268 DDR activation through downregulation of HDAC1 expression.

269 Next, we pharmacologically validated the functional relevance of ATR in HSV-1

replication using Berzosertib, a selective and clinically advanced ATR inhibitor. CCK-8 assays confirmed that the concentration of Berzosertib used (100 nM) did not significantly affect HeLa cell viability or proliferation over 48 hours (Fig. 2K), yet it markedly reduced viral titers in plaque assays (Fig. 2L). Collectively, these findings demonstrate that HSV-1 infection activates the DDR, likely through degradation of HDAC1 and HDAC2 and the resulting histone hyperacetylation. This virus-triggered DDR activation highlights the profound disruption of host chromatin homeostasis and genomic integrity by HSV-1.

HSV-1 promotes the ubiquitin-proteasome degradation of HDAC1/2.

To elucidate the mechanism responsible for HDAC1/2 degradation, we focused on their post-translational regulation. Since HDAC1/2 mRNA levels were unchanged after infection, we hypothesized that the reduction in HDAC1/2 protein is mediated through enhanced proteolytic degradation. To identify the relevant degradation pathway, HSV-1-infected HeLa cells were treated with either the proteasome inhibitor MG-132 or autophagy inhibitors (3-MA and chloroquine). Immunoblotting analysis indicated that only MG-132 rescued HDAC1/2 protein levels (Fig. 3A), confirming that degradation occurs primarily via the proteasomal pathway.

To examine whether HSV-1 infection induced ubiquitination of HDAC1, endogenous immunoprecipitation assays were performed, which revealed increased ubiquitination of HDAC1 following infection (Fig. 3B). Subsequent ubiquitination assays using wild-type (WT), K48-only, and K63-only ubiquitin mutants demonstrated that HDAC1 undergoes K63-linked—but not K48-linked—polyubiquitination (Fig. 3C). Using a series of HDAC1 truncation mutants, we mapped the ubiquitination site to the N-terminal region (amino acids 1–100) (Fig. 3D–F). Site-directed mutagenesis further identified lysine 74 (K74) as the critical residue required for ubiquitination (Fig. 3G–I). Sequence alignment showed that HDAC2 K75 corresponds to HDAC1 K74 (Fig. 3J), and a K75R mutation in HDAC2 similarly abolished ubiquitination (Fig. 3J).

To further validate the role of HDAC1 K74, we first overexpressed HDAC1 WT and HDAC1 K74R and assessed phosphorylation of ATM, ATR, and H2AX; results showed

299 that HDAC1 K74R overexpression suppressed HSV-1–induced DDR signaling(Fig.
300 3K). Furthermore, RT–PCR analysis revealed that overexpression of both HDAC1 WT
301 and HDAC1 K74R inhibited HSV-1 ICP0,ICP8 and gB expression, but HDAC1 WT
302 exerted a significantly stronger inhibitory effect (Fig. 3L). Consistently, HDAC1 K74R
303 overexpression reduced viral titers in plaque assays (Fig. 3M). Together, these results
304 indicate that HSV-1 infection promotes K63-linked polyubiquitination of HDAC1/2 at
305 conserved lysine residues, ultimately leading to their proteasomal degradation.
306 Together, these results indicate that HSV-1 infection promotes K63-linked
307 polyubiquitination of HDAC1/2 at conserved lysine residues, ultimately leading to their
308 proteasomal degradation.
309

310 **MDM2 functions as the E3 ligase mediating HDAC1/2 ubiquitination and**
311 **degradation.**

312 Having established the occurrence of K63-linked ubiquitination (Fig. 3), we next
313 sought to identify the E3 ubiquitin ligase responsible. An RNAi screen targeting
314 candidate E3 ligases revealed MDM2 as the principal mediator of HDAC1/2
315 degradation. Knockdown of MDM2—but not of PIRH2, KCTD11, CHFR, UHRF1, or
316 TRIM46—effectively prevented HDAC1/2 depletion (Fig. 4A, B). Co-IP assay further
317 confirmed an enhanced interaction between HDAC1 and MDM2 following HSV-1
318 infection (Fig. 4C).

319 To characterize this interaction, we focused on the RING finger domain of MDM2,
320 which is essential for its E3 ligase activity. Co-IP analysis demonstrated that HSV-1
321 infection promoted binding between FLAG-HDAC1 and EGFP-MDM2, but not with a
322 RING-deleted mutant (EGFP-MDM2ΔRING) (Fig. 4D), indicating that the interaction
323 was RING domain-dependent. To identify the region within HDAC1 required for
324 binding, HeLa cells were co-transfected with EGFP-MDM2 and either FLAG-HDAC1
325 or the ubiquitination-resistant mutant FLAG-HDAC1 K74R. Infection with HSV-1
326 failed to induce binding between EGFP-MDM2 and the K74R mutant (Fig. 4E),
327 underscoring the essential role of lysine 74 in mediating MDM2-dependent

328 ubiquitination.

329 Ubiquitination assay further revealed that overexpression of EGFP-MDM2ΔRING did
330 not enhance HSV-1-induced ubiquitination or degradation of HDAC1 (Fig. 4F).
331 Similarly, the FLAG-HDAC1 K74R mutant remained resistant to ubiquitination under
332 all experimental conditions (Fig. 4F). To further validate the role of MDM2, we
333 performed MDM2 knockdown in infected cells; RT–PCR analysis showed that MDM2
334 knockdown significantly suppressed HSV-1 *ICP0*, *ICP8*, and *gB* mRNA transcription
335 (Fig. 4G–I), and reduced viral titers in plaque assays (Fig. 4J). Collectively, these results
336 demonstrate that HSV-1 induces HDAC1/2 degradation through MDM2-mediated
337 K63-linked ubiquitination.

338 **HSV-1 triggers cytoplasmic translocation of HDAC1 to facilitate its degradation.**
339 To elucidate the mechanisms by which HSV-1 induces HDAC degradation, we
340 systematically analyzed the subcellular localization of HDAC1. In mock-infected HeLa
341 cells, HDAC1 was predominantly nuclear; however, HSV-1 infection triggered a
342 pronounced translocation of HDAC1 to the cytoplasm (Fig. 5B). This redistribution
343 was completely abolished by treatment with leptomycin B (LMB), a specific inhibitor
344 of CRM1-mediated nuclear export (Fig. 5B). At the same time, CCK-8 assay showed
345 that LMB had no significant effect on cell proliferation (Fig. 5A).

346 To determine whether translocation is functionally linked to degradation, we conducted
347 cycloheximide (CHX) chase assays. Degradation of both HDAC1 and HDAC2 began
348 approximately 12 hours after CHX treatment and was markedly accelerated by HSV-1
349 infection (Fig. 5D). Importantly, LMB treatment restored degradation kinetics to levels
350 comparable to those in mock-infected cells (Fig. 5B). Moreover, under LMB treatment,
351 HSV-1 was unable to induce ubiquitination of endogenous HDAC1 (Fig. 5E). To further
352 validate the subcellular site of HDAC1 ubiquitination, we performed
353 nucleocytoplasmic fractionation followed by immunoblotting; results showed that
354 HSV-1–induced ubiquitination of endogenous HDAC1 occurs specifically in the
355 cytoplasm (Fig. 5F).

356 We further demonstrated that nuclear export and subsequent proteasomal degradation

357 of HDAC1 are strictly dependent on the E3 ubiquitin ligase MDM2. HSV-1 infection
358 induces CRM1-dependent ubiquitination of endogenous HDAC1, thereby establishing
359 CRM1-mediated nuclear export as an essential prerequisite for MDM2-catalyzed
360 HDAC1 degradation (Fig. 5G, H). Consistent with this, immunoblotting analysis
361 revealed that LMB significantly suppressed HSV-1–induced phosphorylation of p53
362 and γH2AX (Fig. 5I). Notably, LMB treatment-by inhibiting CRM1-dependent nuclear
363 export and thereby preventing HDAC1 degradation—markedly impaired HSV-1
364 replication (Fig. 5F). To rigorously test whether HDAC1 nuclear export is the critical,
365 rate-limiting step enabling its ubiquitination and degradation, we employed
366 NESmapper to identify a canonical nuclear export signal (NES) in HDAC1 (residues
367 207–216). We then generated an HDAC1 ΔNES deletion mutant and performed
368 functional rescue experiments in HDAC1-knockdown cells by reconstituting
369 expression of HDAC1 WT, the ubiquitination-deficient mutant HDAC1 K74R, or
370 FLAG-tagged HDAC1 ΔNES. Only HDAC1 WT fully restored the pro-viral phenotype
371 associated with HDAC1 depletion; in contrast, neither HDAC1 K74R nor HDAC1
372 ΔNES rescued viral replication, and both exerted potent antiviral activity—
373 significantly suppressing HSV-1 proliferation relative to controls (Fig. 5K).
374 Collectively, these findings establish that HSV-1 co-opts the CRM1 nuclear export
375 machinery to translocate HDAC1 to the cytoplasm, where it becomes accessible to
376 MDM2 for ubiquitination and subsequent proteasomal degradation, thereby modulating
377 host antiviral defense.

378 **Discussion**

379 HSV-1 manipulates host cellular pathways to facilitate its replication, latency, and
380 reactivation[26]. In this study, we demonstrate that alphaherpesvirus targets class I
381 histone deacetylases HDAC1 and HDAC2 for MDM2-mediated K63-linked
382 polyubiquitination and subsequent proteasomal degradation. This degradation induces
383 histone hyperacetylation, chromatin relaxation, and enhanced viral replication—
384 revealing a mechanism through which alphaherpesvirus reprograms the host epigenetic
385 landscape to optimize viral replication (Fig. 6).

386 In contrast, HSV-1 actively targets HDAC1 and HDAC2 for proteasomal degradation
387 to facilitate lytic replication—a strategy that stands in marked contrast to human
388 cytomegalovirus (HCMV), which relies on HDAC activity to maintain latency[27].
389 This divergence underscores a fundamental difference in epigenetic regulation among
390 herpesviruses. Our data demonstrate that HSV-1–mediated HDAC1/2 degradation
391 initiates as early as 4–6 hours post-infection, coinciding with the onset of immediate-
392 early gene expression and preceding peak viral DNA synthesis. These findings support
393 a context-dependent, dual functional role for HDAC1/2: their enzymatic activity helps
394 enforce transcriptional silencing during latency, whereas their timely removal is
395 essential for chromatin remodeling and efficient lytic gene expression.

396 We identified MDM2[28] as the principal E3 ubiquitin ligase responsible for
397 ubiquitinating HDAC1 at lysine 74 and HDAC2 at lysine 75, leading to their
398 proteasomal degradation. This mechanism is distinct from other E3 ligases, including
399 PIRH2[29] and TRIM46[30]), and critically depends on the RING domain of
400 MDM2[31]. While K63-linked ubiquitination is typically associated with non-
401 proteolytic functions, our work establishes its novel role in mediating HDAC1/2
402 degradation—uncovering a previously unrecognized viral pathogenesis pathway.
403 Targeting this axis using MDM2 inhibitors or inhibiting nuclear export of HDAC1/2
404 significantly restricts viral replication, suggesting that host-directed antiviral strategies
405 may help overcome resistance to direct-acting agents[31].

406 Depletion of HDAC1/2 increases acetylation at histone residues associated with open
407 chromatin and active transcription. Similar chromatin remodeling has been observed in
408 other viral infections[32], underscoring its conserved role in viral gene regulation. Our
409 results are consistent across multiple cell types, including HeLa, 3D4/21, and murine
410 liver, emphasizing the central importance of HDAC1/2 suppression in HSV-1 biology.
411 Notably, HDAC1/2 degradation activates DDR, as indicated by increased γ-H2AX foci
412 and phosphorylation of ATM, ATR, Chk1, and Chk2. This aligns with previous reports
413 that HSV-1 exploits DDR signaling to enhance replication[33-35]. Importantly,
414 HDAC1/2 undergo CRM1-dependent nuclear export prior to degradation—a process

inhibited by leptomycin B—highlighting the essential role of subcellular localization in viral manipulation of host proteins.

HSV-1–mediated HDAC1/2 degradation likely supports viral replication through multiple mechanisms, including evasion of nuclear antiviral sensors and stimulation of viral gene expression. Targeting the MDM2–HDAC1/2 axis represents a promising antiviral strategy. MDM2 inhibitors reduce HSV-1 titers [36], suggesting that modulating ubiquitination pathways could complement existing therapies. Beyond herpesviruses, the MDM2–HDAC axis may be exploited by other DNA viruses that manipulate chromatin and DDR[32], indicating a possible common host vulnerability. However, broad HDAC inhibition may unintentionally enhance viral replication, underscoring the need for targeted therapeutic approaches[37].

This study primarily employed in vitro models (HeLa cells), which lack the neuronal environment essential for studying HSV-1 latency. Future work should validate these findings in primary neurons and trigeminal ganglia [38]. Additional studies are also needed to determine whether HDAC1/2 degradation occurs during reactivation or is limited to lytic infection[7], and to explore the interplay between HDAC degradation, viral tegument proteins, and host stress responses. In vivo evaluation of inhibitors targeting the MDM2/HDAC1–2 pathway will be crucial for assessing their therapeutic potential.

Author contributions

Sheng-Li Ming and Meng-Hua Du : Data curation, Formal analysis, Investigation, Methodology, Validation, Visualization, Writing – original draft; Jia-Ming Yang: Data curation, Formal analysis, Investigation, Validation; Ya-Di Guo: Data curation, Formal analysis, Investigation, Validation, Visualization; Jia-Jia Pan: Data curation, Formal analysis, Investigation, Methodology, Visualization; Wei-Fei Lu: Data curation, Formal analysis, Investigation; Jiang Wang: Methodology, Visualization, Project administration, Supervision, Writing – review & editing; Lei Zeng and Bei-Bei Chu: Conceptualization, Data curation, Funding acquisi-tion, Investigation, Methodology, Project administration, Resources,

Supervision, Validation, Writing – original draft, Writing – review & editing.

Declaration of competing interest

The authors declare that they have no competing interests.

Ethics statement

All procedures involving animals in this study received ethical approval from the Institutional Animal Care and Use Committee (IACUC) of Henan Agricultural University (Permit Number: HNND2020031008). This research was performed in accordance with the regulations specified in the Guide for the Care and Use of Laboratory Animals established by the Ministry of Science and Technology of China

Funding

This research was supported by grants from the National Key R&D Program of China (2021YFD1301200 and 2023YFD1801600), the China Postdoctoral Science Foundation (2025M770267, GZC20240430).

Data Availability Statement

The datas that support the findings of this study are openlyavailable in "Mendeley Data, V3" at https://data.mendeley.com/datasets/yg5fgtvxzk/3, doi: 10.17632/yg5fgtvxzk.3, reference number[39].

Declaration of generative AI and AI-assisted technologies in the writing process

This study affirms that neither generative artificial intelligence nor any other AI-assisted technologies were employed in the preparation of this manuscript.

References

1. Charlotte J, Manale H, Nicky J W, Katherine Me T, Laith J A-R, Sami L G, et al. Herpes simplex virus: global infection prevalence and incidence estimates, 2016. Bull World Health Organ. 2020;98(5). doi: 10.2471/blt.19.237149. PubMed PMID: 32514197.
2. Shu F, Yongzhen L, Yu Z, Zhenfeng S, Zhuxi C, Charles B, et al. Mechanistic insights into the role of herpes simplex virus 1 in Alzheimer's disease. Front Aging Neurosci. 2023;15(0). doi: 10.3389/fnagi.2023.1245904. PubMed PMID: 37744399.
3. Damon J D, Ning Q, Jonathan P G. Neuroinflammation: the devil is in the details. J Neurochem.

478 2016;(0). doi: 10.1111/jnc.13607. PubMed PMID: 26990767.
479 4. S M, Abhimanyu M, D D, P V, P M. Burden of herpes simplex virus encephalitis in the United States.
480 J Neurol. 2017;264(6). doi: 10.1007/s00415-017-8516-x. PubMed PMID: 28516331.
481 5. Saba A, Francesca B. Targeting cyclooxygenases-1 and -2 in neuroinflammation: Therapeutic
482 implications. Biochimie. 2010;93(1). doi: 10.1016/j.biochi.2010.09.009. PubMed PMID: 20868723.
483 6. Orhan A, Oliver U, Carmen I-D, Robert N, Frauke Z. Neuronal damage in brain inflammation. Arch
484 Neurol. 2007;64(2). doi: 10.1001/archneur.64.2.185. PubMed PMID: 17296833.
485 7. David M K, Anna C. Chromatin control of herpes simplex virus lytic and latent infection. Nat Rev
486 Microbiol. 2008;6(3). doi: 10.1038/nrmicro1794. PubMed PMID: 18264117.
487 8. Luis M S, MiYao H, Esteban Flores C, Kairui S. Chromatin-mediated epigenetic regulation of HSV-1
488 transcription as a potential target in antiviral therapy. Antiviral Res. 2021;192(0). doi:
489 10.1016/j.antiviral.2021.105103. PubMed PMID: 34082058.
490 9. Te D, Guoying Z, Shaniya K, Haidong G, Bernard R. Disruption of HDAC/CoREST/REST repressor by
491 dnREST reduces genome silencing and increases virulence of herpes simplex virus. Proc Natl Acad Sci U
492 S A. 2010;107(36). doi: 10.1073/pnas.1010741107. PubMed PMID: 20798038.
493 10. Rui F, Fei C, Zhenghong D, Di H, Andrew J B, Erin A C, et al. LSD2/KDM1B and its cofactor
494 NPAC/GLYR1 endow a structural and molecular model for regulation of H3K4 demethylation. Mol Cell.
495 2012;49(3). doi: 10.1016/j.molcel.2012.11.019. PubMed PMID: 23260659.
496 11. Guoying Z, Te D, Bernard R. HSV carrying WT REST establishes latency but reactivates only if the
497 synthesis of REST is suppressed. Proc Natl Acad Sci U S A. 2013;110(6). doi: 10.1073/pnas.1222497110.
498 PubMed PMID: 23341636.
499 12. Maria S, Asifa A. Modulation of cellular processes by histone and non-histone protein acetylation.
500 Nat Rev Mol Cell Biol. 2022;23(5). doi: 10.1038/s41580-021-00441-y. PubMed PMID: 35042977.
501 13. Patrick L, Joëlle T, Pascale T, Cécile C, Saadi K, Alberto L E. Functional interaction between class II
502 histone deacetylases and ICP0 of herpes simplex virus type 1. J Virol. 2004;78(13). doi:
503 10.1128/jvi.78.13.6744-6757.2004. PubMed PMID: 15194749.
504 14. Georges H, Daniel W. Histone deacetylases in viral infections. Clin Epigenetics. 2010;1(0). doi:
505 10.1007/s13148-010-0003-5. PubMed PMID: 22704086.
506 15. Hao-Ming C, Matthew P, Michelle H, Charles M R, Bryan R G W, Isabelle M, et al. Induction of
507 interferon-stimulated gene expression and antiviral responses require protein deacetylase activity. Proc
508 Natl Acad Sci U S A. 2004;101(26). doi: 10.1073/pnas.0400567101. PubMed PMID: 15210966.
509 16. Isabelle J M, Hao-Ming C, David E L. HDAC stimulates gene expression through BRD4 availability in
510 response to IFN and in interferonopathies. J Exp Med. 2018;215(12). doi: 10.1084/jem.20180520.
511 PubMed PMID: 30463877.
512 17. Inna N, Curt M H. Interferon-stimulated transcription and innate antiviral immunity require
513 deacetylase activity and histone deacetylase 1. Proc Natl Acad Sci U S A. 2003;100(25). doi:
514 10.1073/pnas.2433987100. PubMed PMID: 14645718.
515 18. Amanda J G, Hanna G B, Benjamin A D, Ileana M C. Histone deacetylases in herpesvirus replication
516 and virus-stimulated host defense. Viruses. 2013;5(7). doi: 10.3390/v5071607. PubMed PMID:
517 23807710.
518 19. Sutapa R, Chang L, Tieying H, Istvan B, Allan R B. Requirement of histone deacetylase1 (HDAC1) in
519 signal transducer and activator of transcription 3 (STAT3) nucleocytoplasmic distribution. Nucleic Acids
520 Res. 2008;36(13). doi: 10.1093/nar/gkn419. PubMed PMID: 18611949.
521 20. Xue L, Xiangrong L, Pengpeng H, Facai Z, Juanjuan K D, Ying K, et al. Acetylation of TIR domains in

522 the TLR4-Mal-MyD88 complex regulates immune responses in sepsis. EMBO J. 2024;43(21). doi:
523 10.1038/s44318-024-00237-8. PubMed PMID: 39294473.
524 21. Oriana M, Natalie K H, Laura Z, Silvia C, Richard S, Stefan Z, et al. Inflammation-driven NF-κB
525 signaling represses ferroportin transcription in macrophages via HDAC1 and HDAC3. Blood. 2024;145(8).
526 doi: 10.1182/blood.2023023417. PubMed PMID: 39656097.
527 22. Meiyu S, Xiaoqing Z, Jiamei S, Hongyan D, Xin H, Qiao Y, et al. Saikosaponin b1 Attenuates Liver
528 Fibrosis by Blocking STAT3/Gli1 Interaction and Inducing Gli1 Degradation. Exploration (Beijing).
529 2025;5(5). doi: 10.1002/exp.70000. PubMed PMID: 41163803.
530 23. Prashanth Thevkar N, Matloob H. Influenza A Virus Dysregulates Host Histone Deacetylase 1 That
531 Inhibits Viral Infection in Lung Epithelial Cells. J Virol. 2016;90(9). doi: 10.1128/jvi.00126-16. PubMed
532 PMID: 26912629.
533 24. Jiang W, Guo-Li L, Sheng-Li M, Chun-Feng W, Li-Juan S, Bing-Qian S, et al. BRD4 inhibition exerts
534 anti-viral activity through DNA damage-dependent innate immune responses. PLoS Pathog. 2020;16(3).
535 doi: 10.1371/journal.ppat.1008429. PubMed PMID: 32208449.
536 25. Leong J, Husain M. HDAC1 and HDAC2 Are Involved in Influenza A Virus-Induced Nuclear
537 Translocation of Ectopically Expressed STAT3-GFP. Viruses. 2024;17(1). doi: 10.3390/v17010033.
538 PubMed PMID: 39861822.
539 26. Bernard R, Richard J W. An inquiry into the molecular basis of HSV latency and reactivation. Annu
540 Rev Microbiol. 2013;67(0). doi: 10.1146/annurev-micro-092412-155654. PubMed PMID: 24024635.
541 27. Jane C M, Wolfgang F, Eric V, John H S. Control of cytomegalovirus lytic gene expression by histone
542 acetylation. EMBO J. 2002;21(5). doi: 10.1093/emboj/21.5.1112. PubMed PMID: 11867539.
543 28. R H, H T, H Y. Oncoprotein MDM2 is a ubiquitin ligase E3 for tumor suppressor p53. FEBS Lett.
544 1998;420(1). doi: 10.1016/s0014-5793(97)01480-4. PubMed PMID: 9450543.
545 29. Alexandra D, Olga F, Sergey P, Ivan N, Oleg S, Nickolai A B. The Role of E3 Ligase Pirh2 in Disease.
546 Cells. 2022;11(9). doi: 10.3390/cells11091515. PubMed PMID: 35563824.
547 30. Jicheng T, Xufeng P, Yong C, Yuzhou S, Chunyu J. TRIM46 activates AKT/HK2 signaling by modifying
548 PHLPP2 ubiquitylation to promote glycolysis and chemoresistance of lung cancer cells. Cell Death Dis.
549 2022;13(3). doi: 10.1038/s41419-022-04727-7. PubMed PMID: 35354796.
550 31. Mark W, Yunyuan V W, Geoffrey M W. The p53 orchestra: Mdm2 and Mdmx set the tone. Trends
551 Cell Biol. 2010;20(5). doi: 10.1016/j.tcb.2010.01.009. PubMed PMID: 20172729.
552 32. Lieberman PM. Epigenetics and Genetics of Viral Latency. Cell Host Microbe. 2016;19(5). doi:
553 10.1016/j.chom.2016.04.008. PubMed PMID: 28363823.
554 33. Max E M, David M K. Herpes Simplex Virus 1 Manipulates Host Cell Antiviral and Proviral DNA
555 Damage Responses. mBio. 2021;12(1). doi: 10.1128/mBio.03552-20. PubMed PMID: 33563816.
556 34. Daniel C A, Dipendra G, Kenric A G, William H C, Cary A M. Productive replication of human
557 papillomavirus 31 requires DNA repair factor Nbs1. J Virol. 2014;88(15). doi: 10.1128/jvi.00517-14.
558 PubMed PMID: 24850735.
559 35. Govind A S, Clodagh C OS. Viral and Cellular Genomes Activate Distinct DNA Damage Responses.
560 Cell. 2015;162(5). doi: 10.1016/j.cell.2015.07.058. PubMed PMID: 26317467.
561 36. Shengli M, Shijun Z, Jiayou X, Guoyu Y, Lei Z, Jiang W, et al. Alphaherpesvirus manipulates retinoic
562 acid metabolism for optimal replication. iScience. 2024;27(7). doi: 10.1016/j.isci.2024.110144. PubMed
563 PMID: 38989466.
564 37. James J C, James M M, Douglas R H. Histone deacetylase inhibitors improve the replication of
565 oncolytic herpes simplex virus in breast cancer cells. PLoS One. 2014;9(3). doi:

566 10.1371/journal.pone.0092919. PubMed PMID: 24651853.
567 38. Yue D, Yuqi L, Siyu C, Yuhang X, Hongjia C, Shuyuan Q, et al. Neuronal miR-9 promotes HSV-1
568 epigenetic silencing and latency by repressing Oct-1 and Onecut family genes. Nat Commun. 2024;15(1).
569 doi: 10.1038/s41467-024-46057-6. PubMed PMID: 38443365.
570 39. Sheng-Li Ming M-HD, Jia-Ming Yang, Ya-Di Guo, Jia-Jia Pan, Wei-Fei Lu, Jiang Wang, Lei Zeng, Bei-
571 Bei Chu. The targeted cytosolic degradation of class I histone deacetylases is essential for efficient
572 alphaherpesvirus replication Mendeley Data. 2025. doi: 10.17632/yg5fgtvxzk.3.

573

574

575 **Figure legends**

576 **Figure 1. Viral infection induces degradation of class I HDACs and**
577 **hyperacetylation of histones H3 and H4.**

578 (A) Immunoblotting analysis of the indicated HDACs in HeLa cells infected with HSV-
579 1 (MOI = 1) for the indicated time points.

580 (B) Immunoblotting analysis of the indicated HDACs in 3D4/21 cells infected with
581 PRV-QXX (MOI = 1) for the indicated time points.

582 (C and D) qRT-PCR analysis of *HDAC1* and *HDAC2* mRNA levels, normalized to β-
583 actin expression, in HeLa cells infected with HSV-1 (C) or 3D4/21 cells infected with
584 PRV-QXX (D) (MOI = 1). Data are mean ± SEM; n = 3. $^{**}P < 0.01$, $^{***}P < 0.001$.

585 (E) Immunoblotting of the indicated proteins in HeLa cells from infected with HSV-1
586 (MOI = 1) for the indicated time points.

587 (F) Immunoblotting of the indicated proteins in 3D4/21 cells from infected with PRV-
588 QXX (MOI = 1) for the indicated time points.

589 (G) Immunoblotting analysis of the indicated proteins in liver tissues from mice mock-
590 infected or infected with HSV-1 (1×10^6 pfu per mouse) at 5 days post-infection (n =
591 3).

592 (H) Immunoblotting of the indicated proteins in HeLa cells transfected with siControl
593 or siHDAC1/2.

594

595 **Figure 2. Viral infection triggers chromatin dysfunction and DDR activation via**
596 **HDAC degradation.**

597 (A, B and C) Immunofluorescence staining of γ-H2AX (red) and H2AX (green) in
598 HSV-1-infected HeLa cells (A) or PRV-infected 3D4/21 cells (B) (MOI = 1). Panel C
599 presents the quantitative analysis of γ-H2AX foci intensity or nuclear fluorescence
600 signal derived from panels A and B. Scale bars: 10 μm. Data are mean ± SEM; n =
601 100 cells/group. $^{***}P < 0.001$.

602 (D and E) Comet assay assessing DNA damage in HeLa cells infected with HSV-1
603 (MOI = 1). Data are mean ± SEM; n = 40 cells/group. $^{**}P < 0.01$, $^{***}P < 0.001$.

604 (F and G) Comet assay assessing DNA damage in 3D4/21 cells infected with PRV (MOI
605 = 1) at the indicated time points. Data are mean ± SEM; n = 40 cells/group. $^{**}P < 0.01$,
606 $^{***}P < 0.001$.
607 (H and I) Immunoblotting analysis of DDR markers (p-ATM, p-ATR, p-Chk1, p-Chk2,
608 γ-H2AX) and viral ICP4/EP0 in HSV-1-infected HeLa cells (G) or PRV-QXX-infected
609 3D4/21 cells (H) (MOI = 1).
610 (J) Immunoblotting analysis of DDR markers (p-ATM, p-ATR, γ-H2AX) and
611 HDAC1/HDAC2 in HeLa cells transfected with siHDAC1/2.
612 (K) HeLa cells were treated with vehicle and Berzosertib (0-60 μM) for 0–48 h. Cell
613 proliferation was analyzed by CCK-8 assay. ns, no significance.
614 (L) Viral titers in HSV-1-infected HeLa cells (MOI = 2) treated with berzosertib (50
615 nM) or vehicle. Data are mean ± SEM; n = 3. $^{*}P < 0.05$, $^{**}P < 0.01$, $^{***}P < 0.001$
616 (M) Survival curves of HSV-1-infected mice (1×10^6 PFU/mouse) treated with
617 berzosertib (20 mg/kg) or vehicle (n = 12/group), $^{***}P < 0.001$.
618
619 **Figure 3. Viral infection induces K63-linked ubiquitination of HDAC1/2.**
620 (A) Immunoblotting analysis of the indicated proteins in HeLa cells either mock-
621 infected or infected with HSV-1 (MOI = 1), treated with vehicle, 3-MA (10 μM), MG-
622 132 (10 μM), or chloroquine (10 μM) for the indicated times.
623 (B) Ubiquitination assay of HDAC1 in HeLa cells either mock-infected or infected with
624 HSV-1 (MOI = 1) at 24 hpi.
625 (C) Ubiquitination assay of FLAG-HDAC1 in HeLa cells transfected with HA-
626 ubiquitin variants (WT, K48, K63), and either mock-infected or infected with HSV-1
627 (MOI = 1) at 24 hpi.
628 (D) Schematic representation of HDAC1 deletion mutants.
629 (E-I) Ubiquitination assays of FLAG-HDAC1 mutant variants in HeLa cells either
630 mock-infected or infected with HSV-1 (MOI = 1) at 24 hpi.
631 (J) Ubiquitination assays of FLAG-HDAC2 variants (WT and K75R) in HeLa cells
632 either mock-infected or infected with HSV-1 (MOI = 1) at 24 hpi.
633 (K) Immunoblotting analysis of the indicated proteins in HeLa cells transfected with

634 FLAG-HDAC1 and FLAG-HDAC1 (K74R), and either mock-infected or infected with
635 HSV-1 (MOI = 1) at 24 hpi.
636 (L) qRT-PCR analysis of HSV-1 *ICP0,ICP8* and *gB* mRNA levels, normalized to β-
637 actin expression, in HeLa cells transfected with FLAG-HDAC1 and FLAG-HDAC1
638 (K74R), and either mock-infected or infected with HSV-1 (MOI = 1) at 24 hpi. Data
639 are mean ± SEM; n = 3. ns > 0.05,*P < 0.05,**P < 0.01, ***P < 0.001.
640 (M) Viral titer analysis in HeLa cells transfected with FLAG-HDAC1 or FLAG-
641 HDAC1 (K74R), and either mock-infected or infected with HSV-1 (MOI = 1) at 24 hpi.
642 Data are mean ± SEM; n = 3. **P < 0.01, ***P < 0.001.
643
644 **Figure 4. MDM2 mediates viral-induced HDAC1/2 degradation via K74/K75**
645 **ubiquitination.**
646 (A) qRT-PCR analysis validation of E3 ligase knockdown efficiency (shPIRH2,
647 shKCTD11, shMDM2, shCHFR, shUHRF1, shTRIM46) in HeLa cells. Data are mean
648 ± SEM; n = 3. ***P < 0.001.
649 (B) Immunoblotting analysis of HDAC1/2 stability in E3 ligase-knockdown HeLa cells
650 infected with HSV-1 (MOI = 1).
651 (C) Co-IP assay of endogenous HDAC1-MDM2 interaction in HSV-1-infected HeLa
652 cells (MOI = 1; 24 hpi).
653 (D) Co-IP assay of FLAG-HDAC1 with EGFP-MDM2 (WT or ΔRING) in HSV-1-
654 infected HeLa cells (MOI = 1; 24 hpi).
655 (E) Co-IP assay of FLAG-HDAC1 (WT or K74R) with EGFP-MDM2 in HSV-1-
656 infected HeLa cells (MOI = 1; 24 hpi).
657 (F) Ubiquitination assays of FLAG-HDAC1 (WT or K74R) co-expressed with EGFP-
658 MDM2 (WT or ΔRING) in HSV-1-infected HeLa cells (MOI = 1; 24 hpi).
659 (G-I) qRT-PCR analysis of HSV-1 *ICP0 (H),ICP8 (I)*and *gB (J)* mRNA levels,
660 normalized to β-actin expression, in Scramble and shMDM2 HeLa cells, and either
661 mock-infected or infected with HSV-1 (MOI = 1) at 24 hpi. Data are mean ± SEM; n =
662 3. ns > 0.05,*P < 0.05,**P < 0.01, ***P < 0.001.
663 (J) Viral titer analysis in Scramble and shMDM2 HeLa cells, either mock-infected or

664 infected with HSV-1 (MOI = 2) at 24 hpi. Data are mean ± SEM; n = 3. **P < 0.01,
665 ***P < 0.001.
666
667 **Figure 5. Cytoplasmic translocation enables MDM2-mediated HDAC1**
668 **degradation.**
669 (A) HeLa cells were treated with vehicle and LMB (0-60 μM) for 0–48 h. Cell
670 proliferation was analyzed by CCK-8 assay. ns, no significance.
671 (B and C) Immunofluorescence staining of HDAC1 (red) and viral ICP4 (green) in
672 HSV-1-infected HeLa cells (MOI = 1) ± leptomycin B (LMB; 10 nM; 24 h). Scale bar:
673 10 μm. (C) shows the quantitative analysis of (B), Data are mean ± SEM; n = 100. ***P
674 < 0.001.
675 (D) CHX chase assay measuring HDAC1/2 degradation kinetics in HSV-1-infected
676 HeLa cells (MOI = 1) ± LMB (10 μM).
677 (E) Ubiquitination assay of HDAC1 in HSV-1-infected HeLa cells (MOI = 1) ± LMB
678 (10 μM; 24 h).
679 (F) Immunoblotting analysis of ubiquitination in HDAC1 from cytosolic and nuclear
680 fractions of HeLa cells infected with HSV-1.
681 (G and H) Immunofluorescence analysis of MDM2 (red) and ICP4 (green) in HSV-1-
682 infected HeLa cells (MOI = 1) ± LMB (10 μM; 24 h). Scale bar: 10 μm. (H) shows the
683 quantitative analysis of (G) , Data are mean ± SEM; n = 100. ***P < 0.001.
684 (I) Immunoblotting analysis of DDR markers (γ-H2AX) and HDAC1/2 in HSV-1-
685 infected HeLa cells (MOI = 1) ± LMB (10 μM).
686 (J) Viral titers in HSV-1-infected HeLa cells (MOI = 2) ± LMB (10 μM). Data are mean
687 ± SEM; n = 3. *P < 0.05, **P < 0.01, ***P < 0.001
688 (K) Viral titer analysis in HeLa cells transfected with siHDAC1 transfected with FLAG-
689 HDAC1,FLAG-HDAC1 (K74R) or FLAG-HDAC1 ΔNES, infected with HSV-1 (MOI
690 = 1) at 24 hpi. Data are mean ± SEM; n = 3. **P < 0.01, ***P < 0.001.
691
692 **Figure 6. A schematic model showing the targeted cytosolic degradation of class I**
693 **histone deacetylases is essential for efficient alphaherpesvirus replication.**

694 **Fig .1**

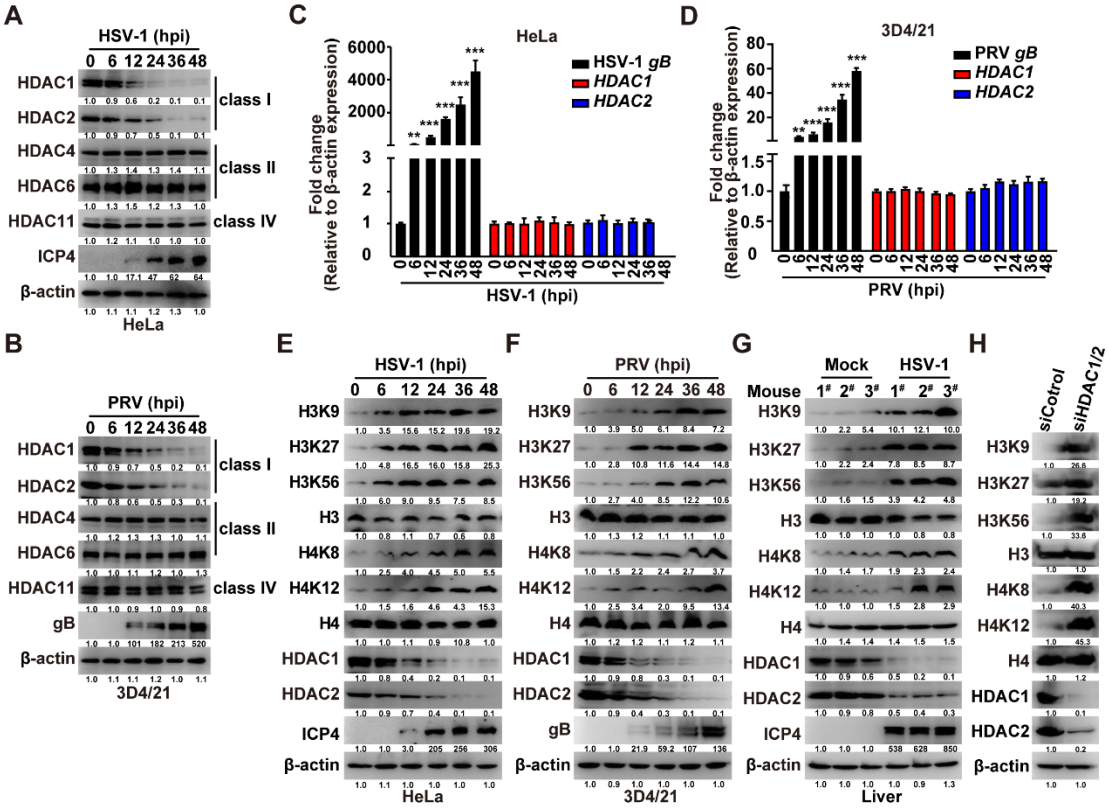

695

696

697

698

Fig .2

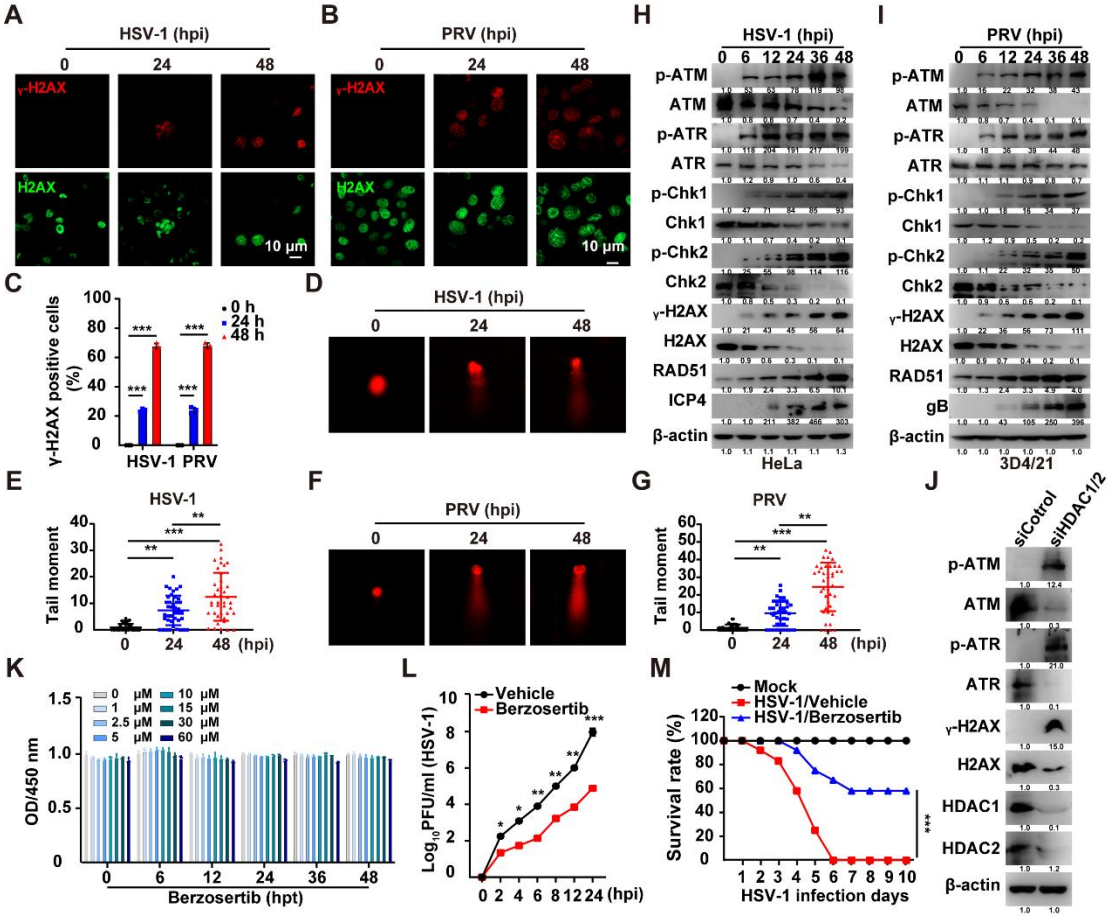
A
HSV-1 (hpi)
0
24
48
γ-H2AX
H2AX
10 μm
B
PRV (hpi)
C
γ-H2AX positive cells (%)
0 h
24 h
48 h
HSV-1 PRV
D
E
HSV-1
Tail moment
(hpi)
F
G
PRV
H
HSV-1 (hpi)
0 6 12 24 36 48
p-ATM
ATM
p-ATR
ATR
p-Chk1
Chk1
p-Chk2
Chk2
γ-H2AX
H2AX
RAD51
ICP4
β-actin
HeLa
I
PRV (hpi)
gB
3D4/21
J
siCotrol
siHDAC1/2
HDAC1
HDAC2
K
OD/450 nm
Berzosertib (hpt)
L
Vehicle
Berzosertib
Log10 PFU/ml (HSV-1)
M
Mock
HSV-1/Vehicle
HSV-1/Berzosertib
Survival rate (%)
HSV-1 infection days

Fig .3

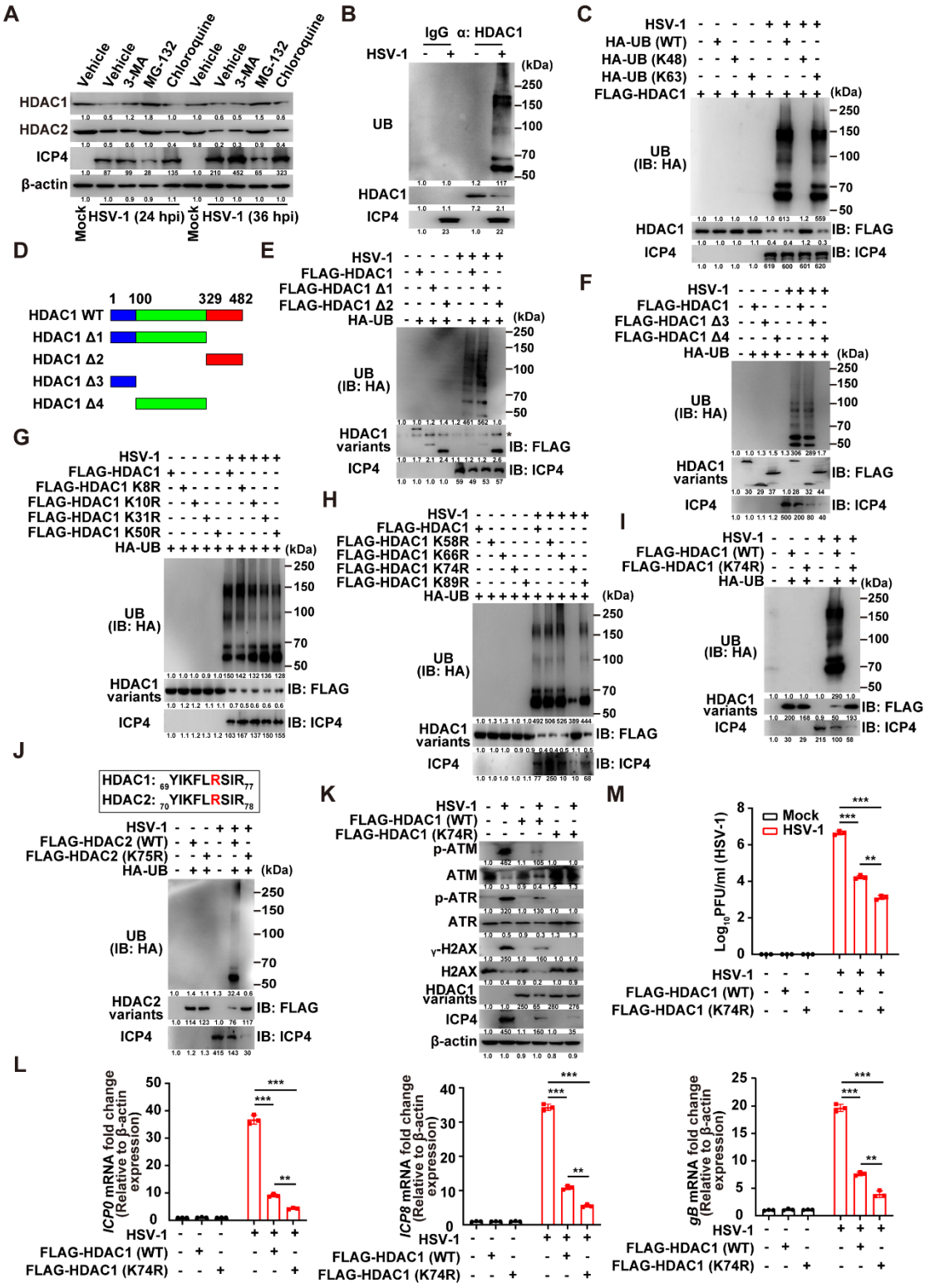
A
Vehicle
Vehicle
3-MA
MG-132
Chloroquine
Vehicle
Vehicle
3-MA
MG-132
Chloroquine
HDAC1
HDAC2
ICP4
β-actin
Mock
HSV-1 (24 hpi)
Mock
HSV-1 (36 hpi)
B
IgG
α: HDAC1
HSV-1
(kDa)
UB
HDAC1
ICP4
C
HSV-1
HA-UB (WT)
HA-UB (K48)
HA-UB (K63)
FLAG-HDAC1
UB (IB: HA)
HDAC1
ICP4
IB: FLAG
IB: ICP4
D
1
100
329
482
HDAC1 WT
HDAC1 Δ1
HDAC1 Δ2
HDAC1 Δ3
HDAC1 Δ4
E
HSV-1
FLAG-HDAC1
FLAG-HDAC1 Δ1
FLAG-HDAC1 Δ2
HA-UB
UB (IB: HA)
HDAC1 variants
ICP4
IB: FLAG
IB: ICP4
F
HSV-1
FLAG-HDAC1
FLAG-HDAC1 Δ3
FLAG-HDAC1 Δ4
HA-UB
UB (IB: HA)
HDAC1 variants
ICP4
IB: FLAG
IB: ICP4
G
HSV-1
FLAG-HDAC1
FLAG-HDAC1 K8R
FLAG-HDAC1 K10R
FLAG-HDAC1 K31R
FLAG-HDAC1 K50R
HA-UB
UB (IB: HA)
HDAC1 variants
ICP4
IB: FLAG
IB: ICP4
H
HSV-1
FLAG-HDAC1
FLAG-HDAC1 K58R
FLAG-HDAC1 K66R
FLAG-HDAC1 K74R
FLAG-HDAC1 K89R
HA-UB
UB (IB: HA)
HDAC1 variants
ICP4
IB: FLAG
IB: ICP4
I
HSV-1
FLAG-HDAC1 (WT)
FLAG-HDAC1 (K74R)
HA-UB
UB (IB: HA)
HDAC1 variants
ICP4
IB: FLAG
IB: ICP4
J
HDAC1: 69YIKFLRSIR77
HDAC2: 70YIKFLRSIR78
HSV-1
FLAG-HDAC2 (WT)
FLAG-HDAC2 (K75R)
HA-UB
UB (IB: HA)
HDAC2 variants
ICP4
IB: FLAG
IB: ICP4
K
HSV-1
FLAG-HDAC1 (WT)
FLAG-HDAC1 (K74R)
p-ATM
ATM
p-ATR
ATR
γ-H2AX
H2AX
HDAC1 variants
ICP4
β-actin
M
Mock
HSV-1
Log10 PFU/ml (HSV-1)
HSV-1
FLAG-HDAC1 (WT)
FLAG-HDAC1 (K74R)
L
ICP0 mRNA fold change (Relative to β-actin expression)
ICP8 mRNA fold change (Relative to β-actin expression)
gB mRNA fold change (Relative to β-actin expression)
HSV-1
FLAG-HDAC1 (WT)
FLAG-HDAC1 (K74R)

Fig .4

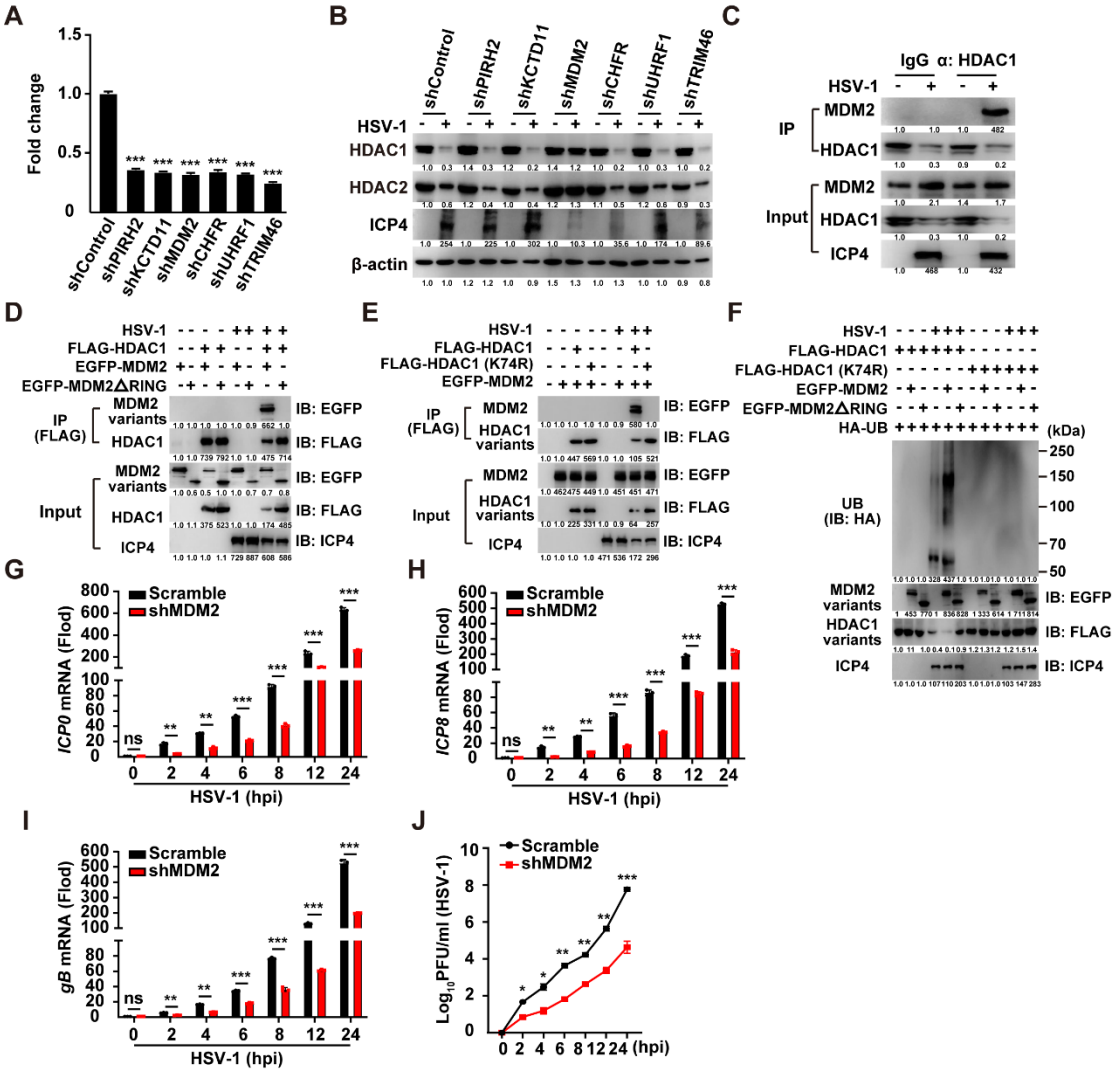
A
Fold change
shControl
shPIRH2
shKCTD11
shMDM2
shCHFR
shUHRF1
shTRIM46
B
HSV-1
HDAC1
HDAC2
ICP4
β-actin
C
IgG
α: HDAC1
IP
Input
MDM2
HDAC1
ICP4
D
HSV-1
FLAG-HDAC1
EGFP-MDM2
EGFP-MDM2ΔRING
IP (FLAG)
Input
MDM2 variants
HDAC1
ICP4
IB: EGFP
IB: FLAG
IB: ICP4
E
FLAG-HDAC1 (K74R)
F
HA-UB
UB (IB: HA)
(kDa)
G
Scramble
shMDM2
ICP0 mRNA (Flod)
HSV-1 (hpi)
H
ICP8 mRNA (Flod)
I
gB mRNA (Flod)
J
Log10PFU/ml (HSV-1)
(hpi)

712 **Fig .5**

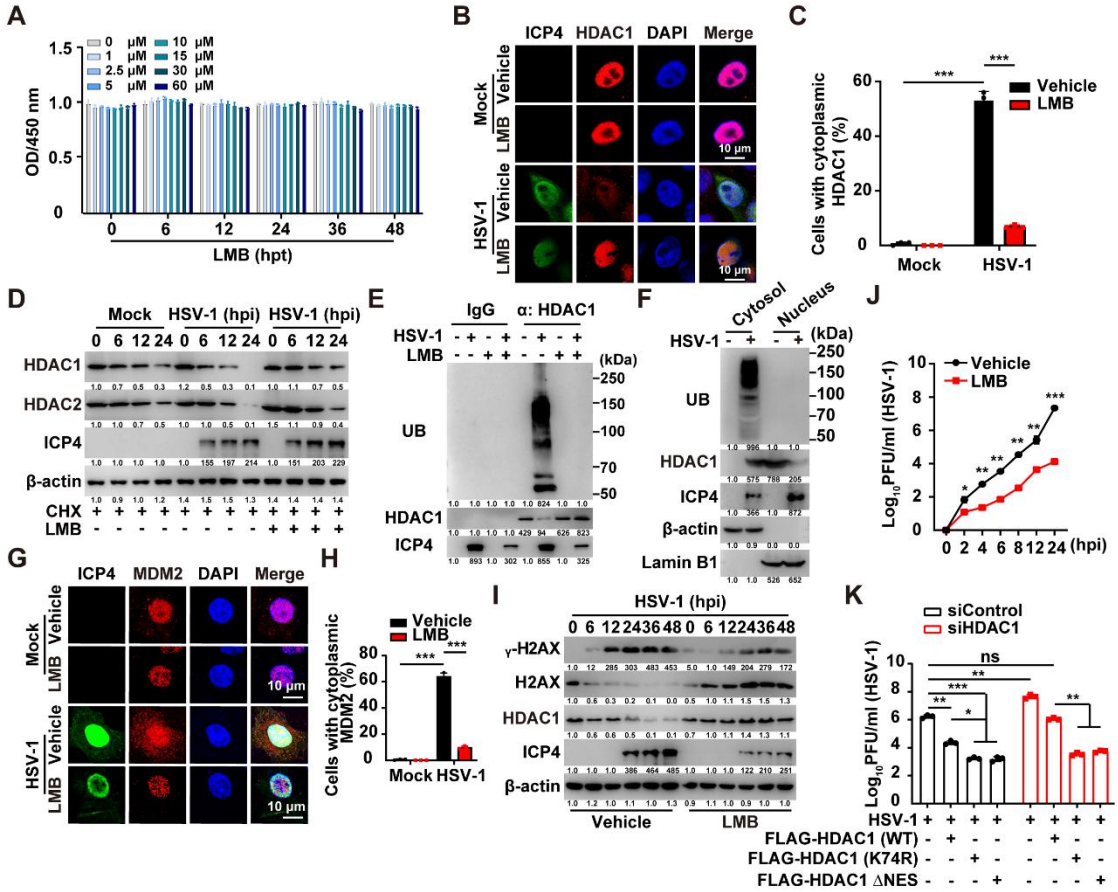

713

714

715

716

717 **Fig .6**

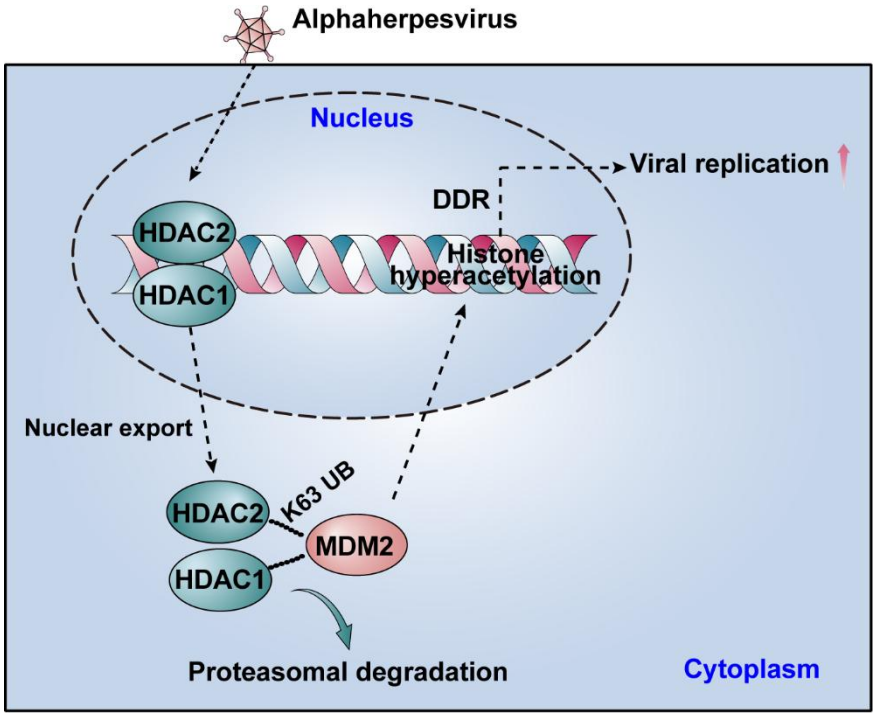

718

719

720

721

722 **Table S1. List of shRNAs and primers used in this study.**

723

Genes	Forward (5′-3′)	Reverse (5′-3′)
Human Q-HDAC1	CATCGCTGTGAATTGGGCTG	CCCTCTGGTGATACTTTAGCAGT
Human Q-HDAC2	TGGCCTTTCTGAGCTGATTT	AGCCACTGAAACAAGACTTCA
Human Q-β-actin	CCTTGCACATGCCGGAG	GCACAGAGCCTCGCCTT
Sus Q-β-actin	CTGAACCCCAAAGCCAACCGT	TTCTCCTTGATGTCCCGCACG
HSV-1-gB	GGACATCAAGGCGGAGAACA	TTCTCCTTGAAGACCACCGC
HSV-1-ICP0	TCTGCATCCCGTGCATGAAAAC	TCACGCCCACTATCAGGTACAC
HSV-1-ICP4	ATCGCATCGGAA AGGGACACG	CCAAGGTGCTTACCCGTGCAA A
siHDAC1	GGCUAGUGUUAUAGAUUAAGC	UUAAUCUAUAACACUAGCCUU
siHDAC2	GGUCAAUAAGACCAGAUAACA	UUAUCUGGUCUUAUUGACCGU
siControl	UUCUCCGAACGUGUCACGUTT	ACGUGACACGUUCGGAGAATT
PRV-gB	CTCGCCATCGTCAGCAA	GCTGCTCCTCCATGTCCTT
Sus Q-HDAC1	TGACGAGTCCTATGAGGCCA	CAAACTCCACACACTTGGCG
Sus Q-HDAC2	CCCCATAAAGCCACTGCTGA	AGCCACCAGTTGAAAGCTGA
Human Q-PIRH2	TATCCTGGGGGAAGGATCGG	TCATGACACAAGCGGCAAGT
Human sh-PIRH2	AATGTAACTTATGCCTAGCTA	TAGCTAGGCATAAGTTACATT
Human sh-KCTD11	GGCACATCCTCAATTTCCTGA	TCAGGAAATTGAGGATGTGCC
Human Q-KCTD11	GATGTAGATGTCAGCCCCCG	GTGCAGAAAAGGTTGGCTCG
Human sh-MDM2	GCCAGAGTGAGTCAGACAAGT	ACTTGTCTGACTCACTCTGGC
Human Q-MDM2	ACCCTGGTTAGACCAAAGCC	TGGCACGCCAAACAAATCTC
Human sh-CHFR	GCAACCAGAGGTTTGACATGG	CCATGTCAAACCTCTGGTTGC
Human Q-CHFR	TGTGTTCCATGGGACCAAAGAT	ACGTCGATGTTGATGGCTGT
Human sh-UHRF1	GCCAGAGTGAGTCAGACAAGT	ACTTGTCTGACTCACTCTGGC
Human Q-UHRF1	AACAGCTCCTGGATCTTCCG	GGTTTCATCGCCATCCCCA
Human sh-TRIM46	GGTGAGGATATGCAGACCTTC	GAAGTCTGCATATCCTCACC
Human Q-TRIM46	ACGGCGAATACAGTGAAG	GCTGGTCCTTGCTGATAG

724

725